Plasma Research Laboratory December, 1965

CHARACTERISTICS OF MAGNETOPLASMAS

SEMIANNUAL STATUS REPORT No. 12

May 1 — October 31, 1965

by E. H. Holt, H. B. Hollinger, D. A. Huchital,
P. Blaszuk and P. N. Y. Pan

Sponsored by the National Aeronautics and Space Administration
under grant no. NsG-48.

Rensselaer Polytechnic Institute
Troy, New York

SUMMARY

16598

Emphasis during this period has been placed on the study of the Kadomtsev instability which pertains to the behavior of a collision dominated plasma in a magnetic field. Work on this instability in the positive column of an electrical discharge in helium has extended the results obtained by other workers to include the effect of a transverse component of the magnetic field. The Kadomtsev theory has been successfully modified to account for the major features of the experimental results.

A further aspect of plasma transport phenomena has been studied. This concerns the initial value aspects of the conduction of heat in a plasma and follows the previous studies dealing with plasma diffusion from this point of view.

A study of the non-Maxwellian form of the electron velocity distribution function in the nitrogen afterglow plasma is reported. This work was done by combining the use of the magnetoplasma waveguide cell, previously developed, with the gated microwave radiometer. The major features of the distribution function in the early afterglow have been revealed. Because of this work the apparently anomalous behavior of the electron gas in the nitrogen afterglow, which was previously reported, has been explained.

Design, construction and the taking of preliminary performance data for various parts of the cesium plasma cell has proceeded. The filament and hot plate structures have been constructed and operated. The design of the probes and the cesium ovens and details of the complete assembly are described.

Author

STUDIES OF ANOMALOUS DIFFUSION ACROSS A MAGNETIC FIELD

The Kadomtsev Instability of the Positive Column

It has been known for some time that many laboratory plasmas will exhibit anomalous effects when immersed in sufficiently strong magnetic fields (1,2). During the present report period a substantial effort was devoted to studies of the positive column of an electrical discharge in helium, immersed in a magnetic field. Emphasis was placed on the study of two aspects of the plasma behavior:

1. The transition from classical to anomalous behavior.
2. The characteristics of the observed anomalous behavior.

Lehnert (3) has observed that a longitudinal magnetic field can enhance the diffusion of a positive column when the field strength exceeds a critical value, B_c. Kadomtsev and Nedospasov (4) explained Lehnert's results by showing that the column becomes macroscopically unstable above a certain value of magnetic field. This work was extended by Cherrington (5), who generalized the treatment of the "Kadomtsev instability" and showed that it can arise whenever gradients exist parallel to a magnetic field in a weakly ionized plasma.

It has been observed in this laboratory and elsewhere (6) that strong, uniform oscillations appear in the positive column when the field strength reaches B_c. Figure 1 shows an example of this behavior as detected by a Langmuir probe inserted into a helium positive column. Increasing the magnetic field strength beyond B_c greatly increases the harmonic content of the oscillation and results in an eventual deterioration into turbulent behavior. The effect of the increased field strength upon the fundamental component of the oscillation is summarized in figure 2. All results obtained to date are qualitatively similar to those of figure 2 regardless of the gas pressure and discharge current.

The Effects of a Transverse Component of Magnetic Field

The Kadomtsev theory describes the effect of a magnetic field which is aligned with the electric field applied to the plasma. A misalignment of the plasma cell in the magnetic field can be described in terms of the presence of a transverse component of the magnetic field. We have studied this effect both theoretically and experimentally.

---

1. Hoh, F. C., Rev. Mod. Phys., 34, 267 (1962).
2. Boeschoten, F., J. Nuc. En., C6, 339 (1964).
3. Lehnert, B., Proc. 2nd U.N. Conf. Peaceful Uses Atomic Energy, 32, 349 (1958).
4. Kadomtsev, B. B. and A. V. Nedospasov, J. Nuc. En., C1, 230 (1960).
5. Cherrington, B. E. and L. Goldstein, Air Force Cambridge Research Laboratories Report, AFCRL 65-257 (1965).
6. Akhmedov, A. R. and A. A. Zaytsev, Soviet Phys., Tech. Phys., 8, 126 (1963).

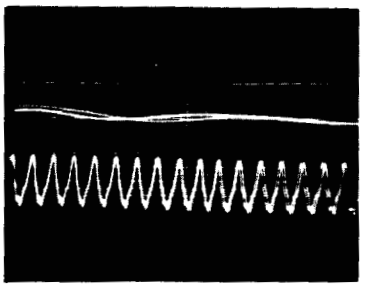

1350 gauss

1380 gauss

Pressure = 0.28 torr

Scales

100 μs/cm horizontal

5 v/cm vertical

FIGURE 1. The Strong Oscillation on a Langmuir Probe which Marks the Transition to Anomalous Behavior for the Positive Column in Helium. The critical magnetic field strength (B_c) is 1380 gauss.

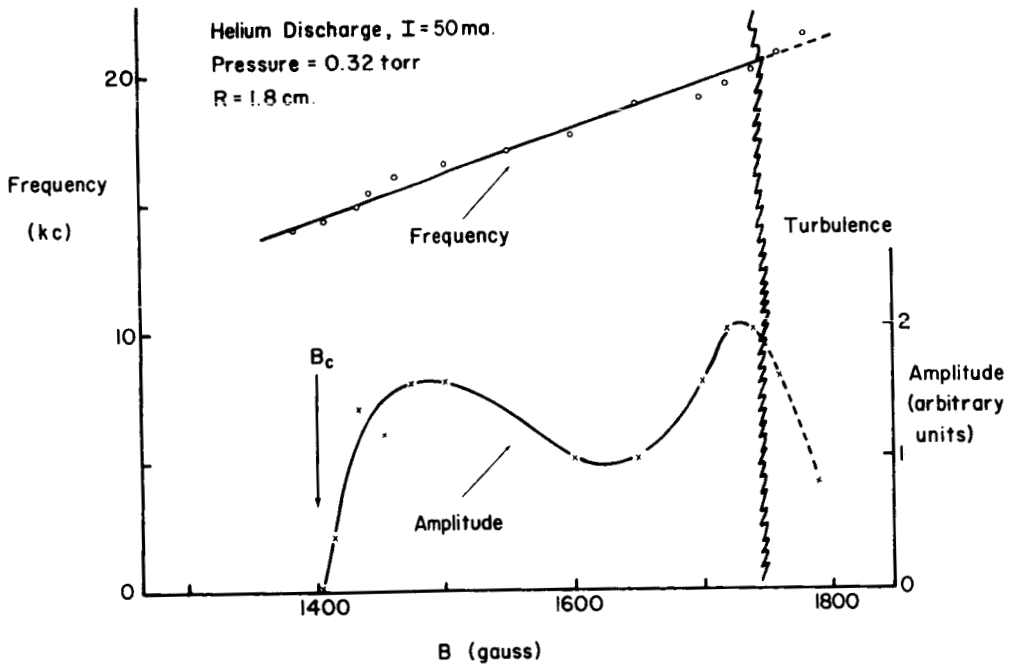

FIGURE 2. Frequency and Amplitude Characteristics of the Strong Oscillation as the Strength of the Magnetic Field is Increased Above the Critical Value (B_c).

Kadomtsev and Nedospasov (4) consider the stability of a screw-shaped perturbation of the plasma density $n(r)$ given by

$$n(r) = J_1(\beta_r) \exp\left[im\phi + i\,kz + i\omega t \right] \qquad (1)$$

where m is an integer and the other symbols have their usual meaning. They then arrive at the following stability criterion

$$Ak^4 + Gk^2 + C \geq m\,D\,\frac{E}{T}\,B \qquad (2)$$

where

E is the electric field along the column
B is the longitudinal magnetic field
T_e is the electron temperature

and

$$A = \frac{1.28 + y}{y(y+1)}\,\gamma^4$$

$$G = \frac{0.8(y+2)}{y}\,\gamma^2$$

$$C = \frac{0.48(1+y)}{y} + 0.1\,\frac{y m^2}{1+y}\,\frac{b_e}{b_i}$$

$$D = 0.163\,\gamma\,\frac{e}{k\,\beta_o}\,\frac{E_z}{T_e}$$

$$y = \frac{b_i}{b_e}\left(\frac{e}{m}\,B\tau\right)^2$$

$$\beta_o = \frac{2.54}{R} \qquad \beta_1 = \frac{3.83}{R}$$

$$\gamma = \frac{k}{\beta_i}\,b_e\,B$$

b_i is the ion mobility

b_e is the electron mobility

R is the radius of the column

t is the electron mean free time

We have modified the derivation of equation (2) to include the effects of a component of the magnetic field which is transverse to the positive column. We obtain the following modified stability criterion:

$$\frac{Ak^4}{P^2} + \frac{Gk^2}{P} + C \geq m \frac{D}{P} \frac{E}{T} B \qquad (3)$$

where

$$P = 1 + (\Omega\tau \tan \theta)^2 \qquad (4)$$

and $\tan \theta$ is the ratio between transverse and longitudinal components of magnetic field.

The criteria can be illustrated graphically as loci in the E/T vs B plane as shown in figure 3. Any combination of E/T and B that falls below a plotted curve is stable; any combination that falls above is unstable. The curves in figure 3 have been calculated for a helium positive column of radius 1.8 cm at a pressure of 0.30 Torr.

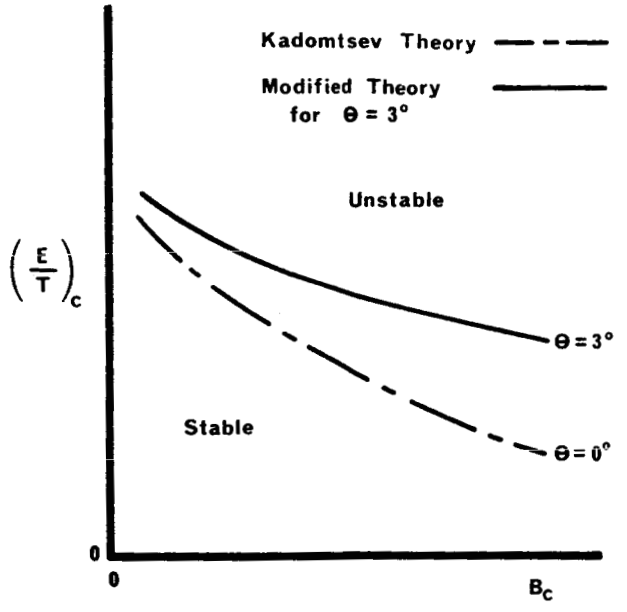

FIGURE 3. The Stability Criterion for a Positive Column Showing the Effect of a Transverse Component of the Magnetic Field. ($\tan \theta = B_{transverse}/B_{longitudinal}$)

It is apparent that the plasma is more stable for $\theta = 3^{\circ}$ than for $\theta = 0^{\circ}$ and, in fact, a general conclusion of the theoretical analysis is that the region in which the plasma is stable increases in size as θ increases. This phenomenon is explained by the fact that the electron mobility along the column is sharply reduced for $\theta > 0$. In this manner the transverse magnetic field inhibits the space charge separation that drives the instability.

In order to determine the onset of the instability, it is necessary to consider the experimental locus of the parameter E/T as a function of B in a given discharge (figure 4). The point where this locus crosses the stability curve determines the critical values of the magnetic and electric fields. In a given discharge it is found experimentally that E/T decreases monotonically with B for $\theta = 0^{\circ}$. This is due to the reduction in the value of the ambipolar diffusion coefficient across the magnetic field. However, for $\theta > 0$, E/T increases with B because of the presence of a force due to the cross product of E and $B_{transverse}$ which leads to increased plasma losses. Thus a larger electric field is required to maintain the plasma which results in a larger value of E/T because the electron temperature (T) is relatively insensitive to these effects (7).

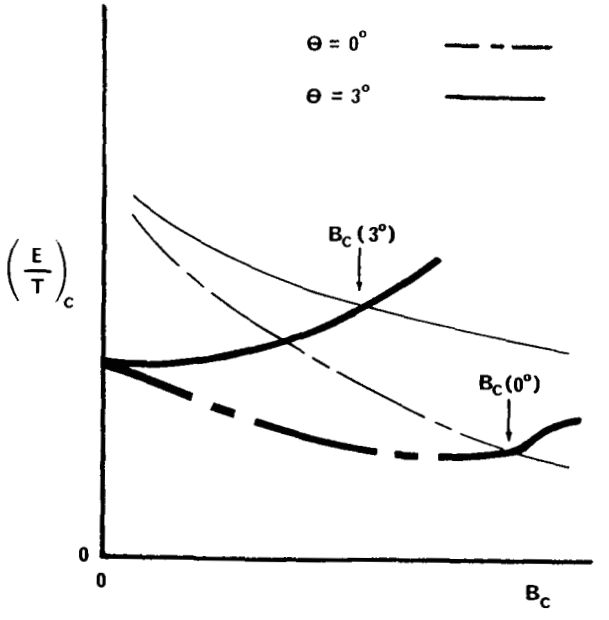

FIGURE 4. Experimental Locus of E/T vs. B for a Given Discharge Showing the Point at which the Locus Crosses the Stability Curve.

---

7. Beckman, L., Proc. Phys. Soc., 61, 515 (1948).

From figure 4 we can draw the conclusion that for a given discharge the critical electric field will be higher and the critical magnetic field will be lower when θ is changed from 0° to 3°. Figure 5 provides experimental justification of this point in the form of a plot of potential along the column versus longitudinal magnetic field. Data are presented for several values of θ. The critical points for onset of the instability are indicated by arrows. Figure 6 shows how the value of the critical magnetic field depends on the angle θ for a number of gas pressures. As expected, B_c decreases significantly with increasing θ.

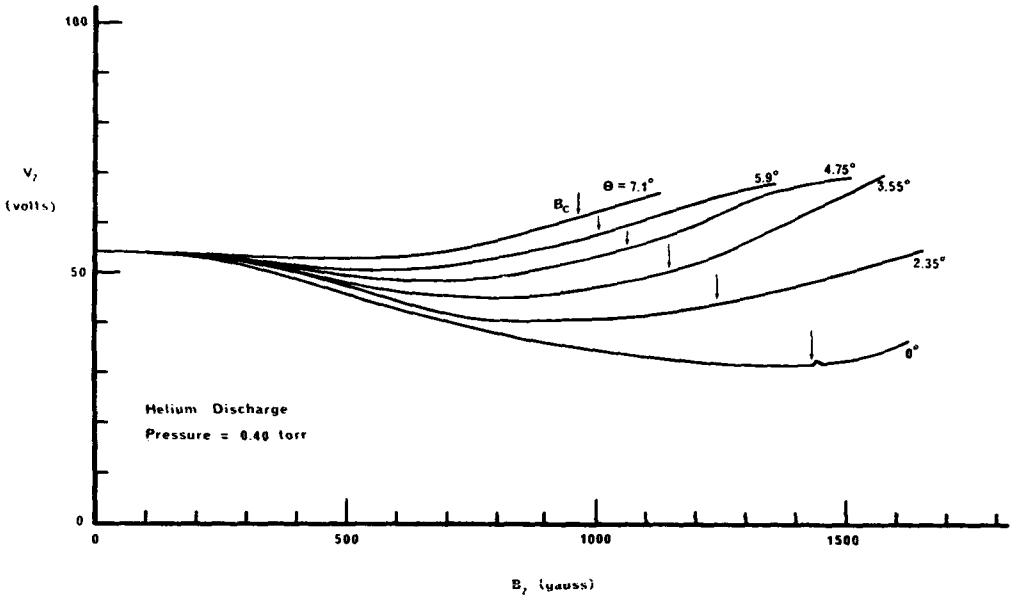

FIGURE 5. Variation of the Potential Along the Positive Column (V_z) as a Function of the Longitudinal Component of the Magnetic Field (B_z) for Various Values of θ. The arrows show the values of the longitudinal component of the critical magnetic field.

The modified stability criterion has been subjected to a computer analysis with the following results:

(i) As θ increases, the frequency of oscillation of the instability is predicted to increase.

(ii) The $m = 1$ perturbation (see equation 1) is the least stable at $\theta = 0^{\circ}$ and is therefore the first instability to appear. When θ increases, the $m = 2$ instability should dominate. The instability mode change from $m = 1$ to $m = 2$ should be evidenced by a sudden change in oscillation frequency and a change in the character of the B_c vs. θ curve.

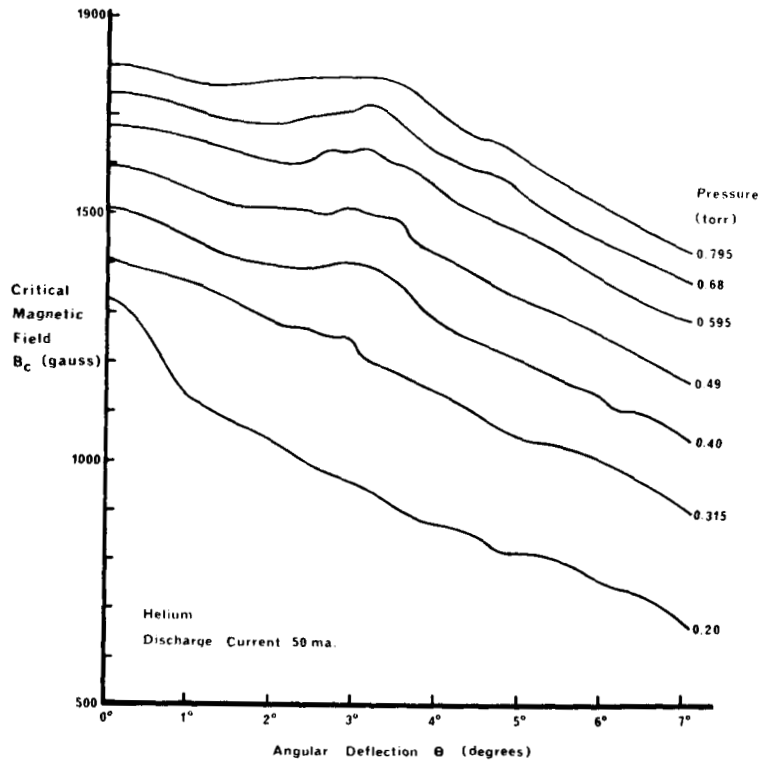

FIGURE 6. Dependence of Critical Magnetic Field (B_c) upon the Angle θ.

These predictions are substantiated by the experimental results shown in figure 7, which shows the observed oscillation frequency as a function of θ for various pressures. It should be noted that the vicinity of the $m = 2$ discontinuity corresponds to the slight irregularities apparent in the B_c vs. θ curves shown in figure 6.

HEAT CONDUCTION IN PLASMA

Previous work (8) on plasma diffusion is being extended to heat conduction. This is a continuation of the study of transport phenomena in plasmas. The problem is that the traditional description in terms of linear transport laws and transport coefficients is not appropriate, conceptually, in a fluctuating or rapidly varying external force field, or during the early stages of an irreversible process.

---

8. Huchital, D. A. and E. H. Holt, Plasma Diffusion as an Initial Value Problem, Plasma Research Laboratory, Rensselaer Polytechnic Institute, Technical Report No. 15, December, 1964.

   Huchital, D. A. and E. H. Holt, Paper 4.2.2(4), 7th International Conference on Phenomena in Ionized Gases, Belgrade, 1965.

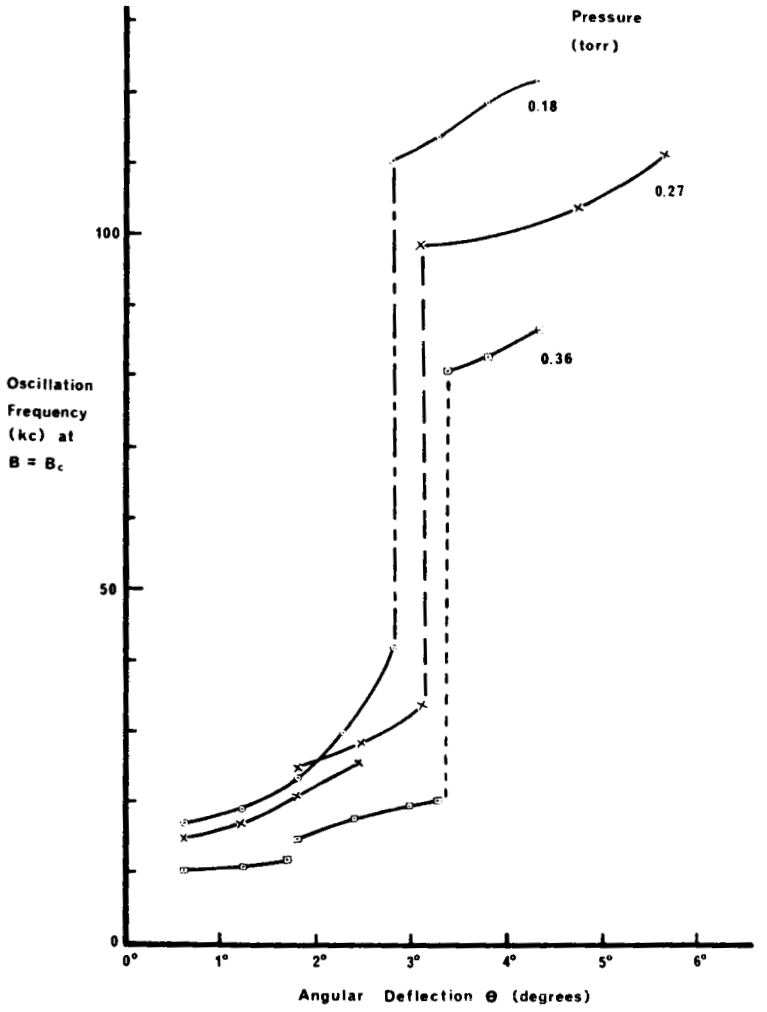

FIGURE 7. Variation of Oscillation Frequency at $B = B_c$ as a Function of the Angle θ.

If heat conduction is described in the traditional way, then the heat flux vector $\underline{q}$ is related to the gradient of temperature ∇T and the heat conductivity λ by the following equation:

$$\underline{q} = - \lambda \nabla T \tag{5}$$

and the time-dependence of the state of the fluid is governed by

$$\frac{\partial}{\partial t} T = \frac{\lambda}{c} \nabla^2 T \tag{6}$$

Equation (5) can be generalized by the method of irreversible thermodynamics (9) to include contributions to the heat flux due to gradients in other properties, and it can be generalized to include effects of internal structure. The transport coefficients can be related to particle parameters by the method of

9. DeGroot, S. and P. Mazur, Non-equilibrium Thermodynamics, North Holland Publishing Company, Amsterdam, 1962. Chapter 11.

kinetic theory (10). Equations (5) and (6) with these generalizations constitute the present theory of heat conduction, whether in plasma or other materials. This theory is quite limited conceptually as it is built upon eqs. (5) and (6), which cannot take account of arbitrary initial conditions. In spite of this, the theory has been quite successful in applications to fluids. The framework of the theory has been carried over intact to the study of plasma (10,11), and the treatment of heat conduction in plasma has been a matter of determining parameters in the traditional description (10,11,12). Although the description has been modified to take into account the long-range interactions of charged particles (11), and experiments have been developed in which coupling with other processes is suppressed (12), there has been no attempt to challenge the form of the description based on equations (8) and (9) in a manner analogous to that which we have applied to diffusion (8). Our purpose then is to generate a more general description of heat conduction in plasmas and to determine under what circumstances it predicts important deviations from the traditional theory.

In the first approximation, the theoretical approach to the description of heat flow from an initial state in which there is local heating of electrons can be developed from the Boltzmann equation in the form

$$\frac{\partial}{\partial t} f + \underline{v} \cdot \frac{\partial}{\partial \underline{r}} f + \underline{R} \cdot \frac{\partial}{\partial \underline{v}} f = J_{EN} \tag{7}$$

where $f(\underline{r}, \underline{v}, t)$ is the density of electrons in the phase space of positions and velocities, $(\underline{r}, \underline{v})$, $\underline{R} = (e/m)(\underline{E} + \underline{v} \times \underline{B})$ is the external force per unit mass acting on the electrons, and J_{EN} is the collision integral for electron-neutral collisions. If we introduce a perturbation expansion that emphasizes the collisions in the lowest approximation, we obtain the traditional description of transport phenomena -- which is not appropriate in an arbitrary, non-equilibrium state. If we introduce the expansion of f in spherical harmonics on velocity space, we obtain the description which has been used to emphasize initial conditions in the description of diffusion (8). Following this latter course, we write

$$f = \sum_{\ell=0}^{\infty} \sum_{m=\ell}^{\ell} f_{\ell m}(\underline{r}, v, t)\, Y_{\ell m}(\theta, \phi) \tag{8}$$

where the $Y_{\ell m}$ are the spherical harmonics. Putting (8) into (7) and using the orthogonality properties of the spherical harmonics, we obtain a hierarchy

---

10. Chapman, S. and T. G. Cowling, Mathematical Theory of Non-Uniform Gases, Cambridge, 1952.

11. Spitzer, L. and R. Harm, Phys. Rev. 89, 977 (1953); L. Spitzer, Physics of Fully Ionized Gases, Interscience, New York, 1953.

12. Goldstein, L. and T. Sekiguchi, Phys. Rev. 109, 625 (1958); Sekiguchi, T. and R. C. Herndon, Phys. Rev. 112, 1 (1958).

of coupled equations for the coefficients in eq. (8):

$$\left(\frac{\partial}{\partial t} + im\Omega + \nu_\ell\right) f_{\ell m} = - \sum_{L=\ell-1}^{\ell+1} \sum_{M=m-1}^{m+1} K(\ell, m; L, M)\, f_{LM} \qquad (9)$$

where Ω is eB/m and

$$\nu_\ell = v \int dv_N \int d\omega\, S(\chi) \left[1 - P_\ell(\cos\chi)\right] f^N \qquad (10)$$

in which S is the scattering cross section, P is a Legendre polynomial, and f^N is the density of neutrals in the one-particle phase space. The coefficients $K(\ell, m; L, M)$ in (9) are the operators:

$$K(\ell, m; \ell, M) = 0 \quad \text{for any } M$$

$$K(\ell, m; \ell-1, m \pm 1) = \pm B(\ell, \mp m) \left[-\varepsilon_\pm \left(\frac{\ell-1}{v} - \frac{\partial}{\partial v}\right) - v \frac{\partial}{\partial r_\mp}\right]$$

$$K(\ell, m; \ell+1, m \pm 1) = \pm B(\ell+1, \pm m + 1) \left[-\varepsilon_\pm \left(\frac{\ell+2}{v} + \frac{\partial}{\partial v}\right) + v \frac{\partial}{\partial r_\pm}\right]$$

$$K(\ell, m; \ell+1, m) = A(\ell+1, m) \left[v \frac{\partial}{\partial z} - \varepsilon_z \left(\frac{\partial}{\partial v} + \frac{\ell+2}{v}\right)\right]$$

$$K(\ell, m; \ell-1, m) = A(\ell, m) \left[v \frac{\partial}{\partial z} - \varepsilon_z \left(\frac{\partial}{\partial v} - \frac{\ell-1}{v}\right)\right] \qquad (11)$$

where

$$\varepsilon_\pm = \frac{e}{2m} (E_x \pm iE_y) \qquad \varepsilon_z = \frac{e}{m} E_z$$

$$r_\pm = x \pm iy$$

$$A(\ell, m) = \sqrt{\frac{(\ell - m)(\ell + m)}{(2\ell - 1)(2\ell + 1)}}$$

$$B(\ell, m) = \sqrt{\frac{(\ell + m)(\ell + m - 1)}{(2\ell - 1)(2\ell + 1)}} \qquad (12)$$

These equations can be used to find an approximate formula for f, which can then be used to predict the variation of temperature from arbitrary initial conditions without appealing to the linear Fourier law for heat flow. Errors in the prediction would grow with time, for this treatment emphasizes early stages of the irreversible process, but it should be possible to determine

whether there is quick relaxation to traditional heat flow.

This approach to the description of heat flow would make use of all of the data obtained in experiments like those of reference 12. By contrast, the interpretation of those data in terms of the traditional description makes minimal use of the data.

CESIUM PLASMA GENERATOR

Further design and construction of the cesium plasma cell has progressed in the following areas:

1. The electron gun assembly has been completed and is now undergoing preliminary performance tests.

2. The design of the neutral plasma region has been completed.

3. Diagnostics techniques have been investigated.
   a. Specially designed Langmuir probes have been constructed.
   b. The use of microwave measurements has been explored.

4. The power supplies necessary to drive the electron gun assembly have been built and tested.

The two major design criteria which have been followed are the attainment of high equilibrium plasma density and the demountability of the major components of the generator. The most important feature of the design as regards the first criterion is the use of independent vacuum chambers for housing each of the two filaments. These provide the electrons used to heat the tantalum plates which ionize the cesium atoms on contact.

The dimensions of the cell lead to the prediction of an ultimate plasma density of between 10^{14} and 10^{15} charged particles per c.c. Figure 8 shows the relationship between the expected plasma density and the collector temperature.

Electron Gun Assembly

A figure from the previous status report is reproduced here (figure 9) for comparison with the present electron gun assembly (figure 10). The design shown is completely demountable and consists of three sections; the enclosure, the filaments, and the collector.

The Enclosure

The enclosure is composed of FN glass, Kovar metal, and a standard Varion flange. Two tungsten rods, 80 mils. in diameter, are fixed in a glass press arrangement and have female connectors brazed to them.

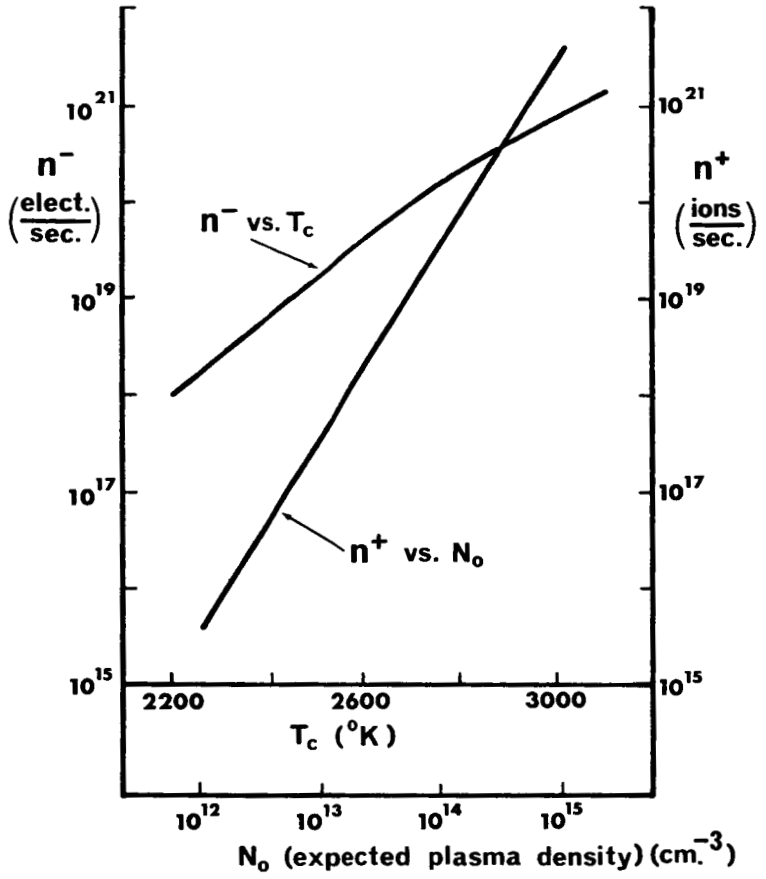

FIGURE 8. Relationship between the Expected Plasma Density in the Cesium Plasma Generator and the Collector (Hot Plate) Temperature. These quantities are shown as functions of the rates of positive ion generation and electron emission respectively.

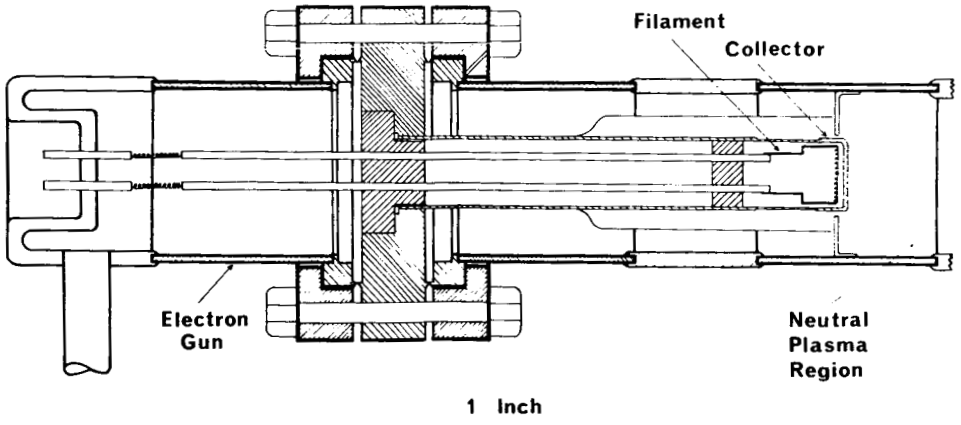

FIGURE 9. Electron Gun Assembly. The original design as shown in the previous status report.

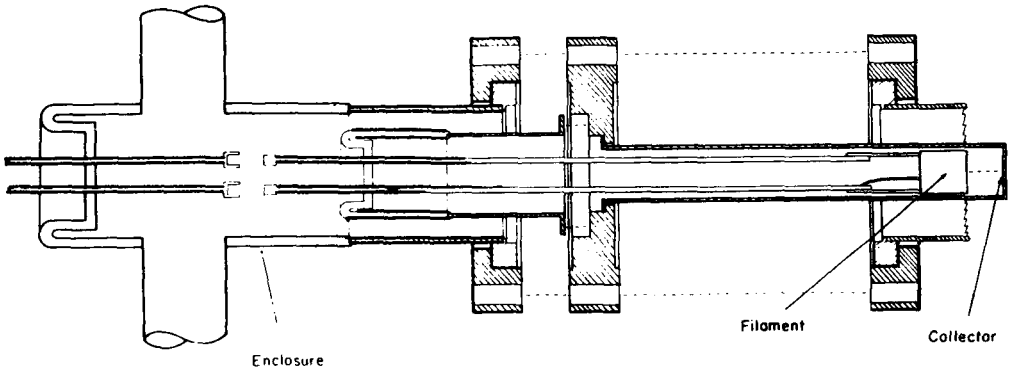

FIGURE 10. Expanded View of the Electron Gun Assembly as Finally Constructed.

The Filament Region

The filament region consists of 2 tantalum rods, 80 mils. in diameter, fixed in a second glass press with appropriate vacuum pumping holes. This glass press is sealed to a kovar spinning as shown which is screwed directly to the center flange. A tungsten filament 25 mil. in diameter is attached to the ends of the tantalum rods and enclosed by a cylindrical heat shield, which is held at the same potential as the filaments.

The Collector

Since cesium has an ionization potential of 3.87 ev., the collector material must have a work function greater than this value. Two materials were considered, tungsten (4.52 ev.) and tantalum (4.19 ev.). We chose tantalum for the following reason. Tungsten is a refractory metal with a melting point of 3668°K. This makes it necessary to employ special fabrication techniques. Tantalum on the other hand, is a very ductile material with a melting point of 3270°K. It exhibits a low vapor pressure at high temperatures and is extremely corrosion resistant.

The collector has a cylindrical shape, 600 mil. in diameter, 20 mil. wall thickness, and 3.5 inches long. A reduction in the wall thickness to 10 mil. for a length of 1/2 inch is employed to induce a temperature gradient along the length of the collector. This, in effect, maintains high temperatures at the collector end while the filament end is cool.

Neutral Plasma Region

A schematic of the design of the neutral plasma region of the generator is shown in figure 11. The sections containing the cesium plasma sources are under construction as is the fixed probe. The microwave cavity, the moveable probe and the ceramic insulating sections are still in the design stage.

Commercially available ultra high vacuum components are used in the form of crosses and flanges as shown. Thus the design is highly flexible and may be readily modified.

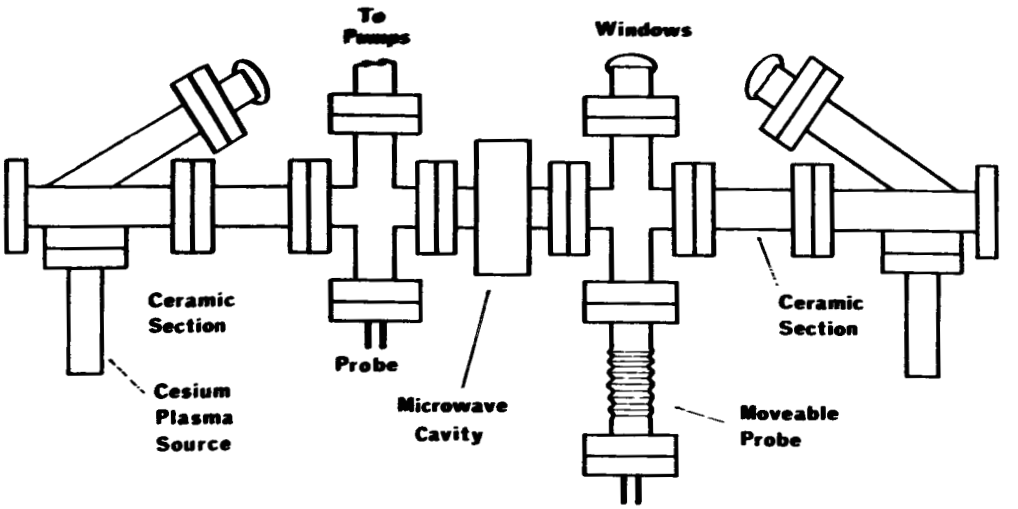

FIGURE 11. Schematic Diagram of the Neutral Plasma Region of the Cesium Plasma Generator.

The Cesium Plasma Sources

These are shown in figure 12 and each consist of a cesium reservoir and a viewing port which are shown in relation to the electron collector and hot plate, which is part of the electron gun assembly described above.

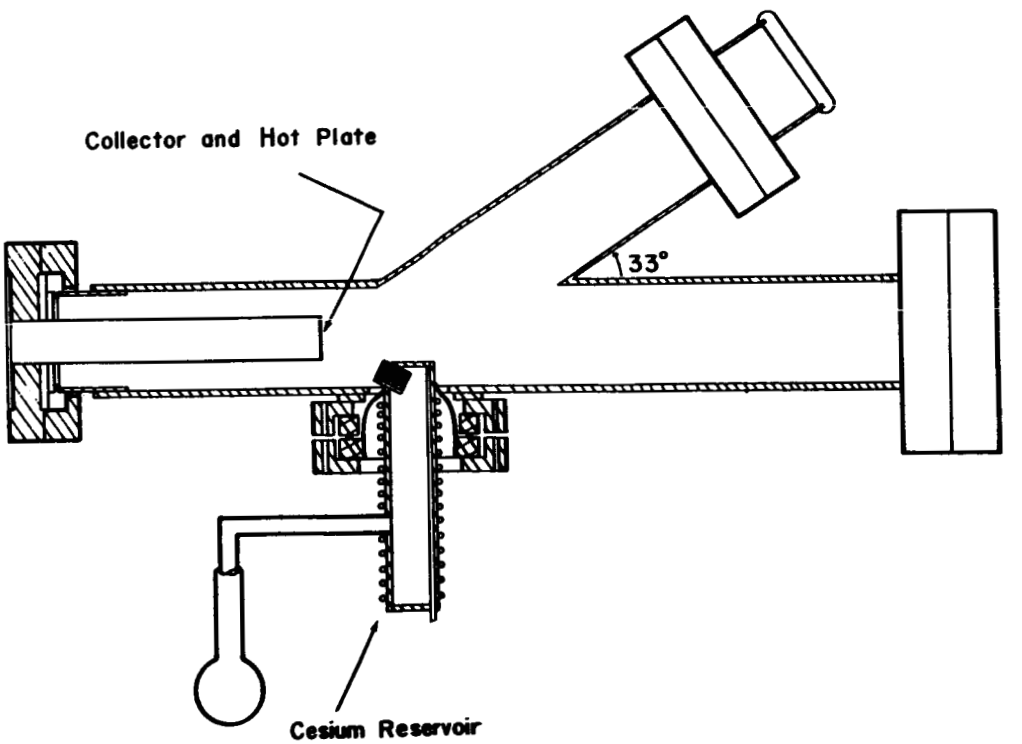

FIGURE 12. Cesium Plasma Source. The cesium reservoir, viewing port and hot plate from the electron gun assembly are shown.

The cesium reservoir acts to collimate the cesium atoms into a beam and then direct this beam towards the collector surface. Collimating action is accomplished by the use of 1000 stainless steel rods 7 mils. inner diameter and 1 1/4 inches long. The design criterion is such that the diameter of the rods is less than the mean free path of the cesium atoms at the optimum densities to be used. Amperex heater wire is brazed to the reservoir to insure accurate control of the temperature and hence the vapor pressure of the cesium. Cesium is introduced into the reservoir by heating the pyrex container as shown and cooling the reservoir. Once the cesium has been driven into the reservoir, the glass is drawn off under vacuum. The cesium reservoir is attached to the main tube by means of an ultra high vacuum flange.

The glass viewing ports are made of FN glass attached to the flanges by means of oxide free seals. They are used for making temperature measurements of the collector using an optical pyrometer.

Diagnostic Techniques

Two principle diagnostic techniques are being developed. Fixed and moveable Langmuir probes on the one hand and a microwave cavity device on the other.

Langmuir Probes

The general features of the construction and electrical connections of the Langmuir probes which have been built, but not tested as yet, are shown in figure 13.

A specially constructed probe is necessary when alkali vapors are used as the plasma medium. This was pointed out by Bullis in 1960 (13). Plasma augmentation of the surface conductivity of conventionally insulated probes is examined in detail by Fowler and Sakuntala (14). The probe construction consists of 5, 10, or 20 mil. tungsten wire spot welded and wrapped onto a 60 mil. tungsten rod. This is then coated with a 15 mil. layer of high density alumina, a 15 mil. layer of tungsten metal, and an outer jacket of high density alumina (15 mil.). The coating of tungsten is electrically connected to act as a guard ring and the collection of plasma particles occurs only at the probe tip.

---

13. Bullis, R. H., J. Adv. Energy Conversion, 1, 1 (1960).

14. Fowler, R. G. and M. Sakuntala, J. Chem. Phys. 27, 824 (1957).

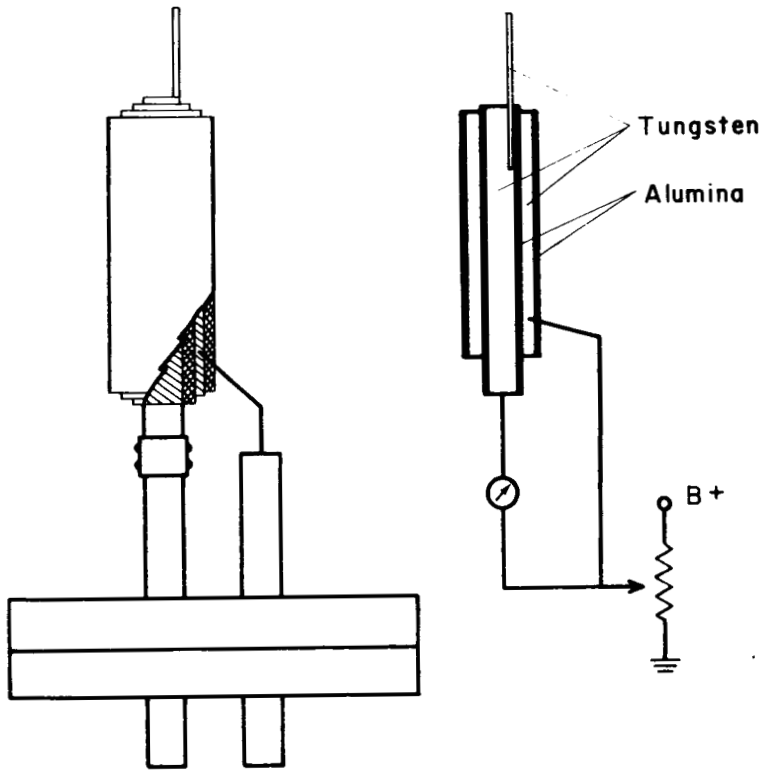

FIGURE 13. Langmuir Probe Construction and Electrical Connections.

Power Supplies

The filament power supplies have been designed and built to produce a maximum output of 20 volts at 40 amps. with ripple less than 0.5%. They operate with either terminal grounded or both output terminals floating at a maximum potential of 2500 volts above or below ground. The power utilizes an active solid state filter network and a diode bridge rectifier.

The collector power supplies have been designed and built to produce a maximum output of 3000 volts at 800 ma. continuous operation with a ripple less than 1%. They employ positive or negative ground, or both terminals may float at a maximum of 5000 volts above or below ground. The power supply employs a three section LC filter network and a diode bridge rectifier circuit.

THE ELECTRON VELOCITY DISTRIBUTION FUNCTION IN MAGNETOPLASMAS

The magnetoplasma cell (15) in the bakable version which was described in the last report has been used in a study of the form of the electron velocity distribution function in the afterglow of a nitrogen plasma. This work extends the previous work on the nitrogen afterglow (16). The gated, microwave radiometer (17) has been used again to measure the radiation temperature of the electron gas constituent of the plasma. However with the addition of a magnetic field it has been possible to adapt a technique used to analyze steady state plasmas (18) which provides information about the form of the electron velocity distribution function.

Fields, Bekefi and Brown (18) have shown that the radiation temperature T_r of a plasma can be written in terms of the electron velocity distribution function as follows:

$$T_r = -\frac{1}{k} \frac{\int_o^\infty \frac{\nu(v)}{\nu^2(v) + (\omega - \omega_b)^2} f(v)\, v^4\, dv}{\int_o^\infty \frac{\nu(v)}{\nu^2(v) + (\omega - \omega_b)^2} \frac{\partial f(v)}{\partial U}\, v^4\, dv} \qquad (13)$$

where $\nu(v)$ is the electron-neutral collision frequency which is a function of the electron velocity v.

ω is the frequency of the radiation

ω_b is the cyclotron frequency

U is the electron energy

k is the Boltzmann constant

If the form of the electron velocity distribution function $f(v)$ is approximated by

$$f(v) \propto \exp(-bv^{\ell})$$

and $\nu(v)$ is written in terms of the collision cross section σ_d as $\nu = \sigma_d P_o v$ where P_o is the reduced pressure ($P_o = 273\ P/T$), equation (13) can be written as

---

15. Noon, J. H., E. H. Holt and J. F. Reynolds, Rev. Sci. Instr. 36, 622 (1965).
16. Stotz, K. C. NASA TN D-2226 (1963) and J. H. Noon, E. H. Holt and J. P. Quine, Bull. Amer. Phys. Soc. 10, 185 (1965).
17. Taft, W. C., K. C. Stotz and E. H. Holt, IEEE Trans. IM-12, 90 (1963).
18. Fields, H., G. Bekefi and S. C. Brown, Phys. Rev. 129, 506 (1963).

$$T_r = \frac{m}{kb\ell} \frac{\int_0^\infty \frac{\sigma_d(v)}{\sigma_d^2(v) + \Delta K/v^2} \exp(-bv\ell) v^3 \, dv}{\int_0^\infty \frac{\sigma_d(v)}{\sigma_d^2(v) + \Delta K/v^2} \exp(-bv\ell) \, v^{\ell+1} \, dv} \tag{14}$$

where $\Delta K = (\omega - \omega_b)^2/P_o^2$ and $K = 10^{16}$

m is the electron mass

In order to solve equation (14) by numerical computation we have quantized the collision frequency over appropriate velocity ranges. Thus we write

$$\nu = A_i P_o \quad \text{for} \quad v_i \leq v \leq v_{i+1} ,$$

the value of A_i depending on the range of v. Finally, the use of incomplete factorial functions permits equation (14) to be written as

$$T_r = \frac{1}{k\ell b^{2/\ell}} \frac{\sum_{i=0}^{n} \frac{A_i}{A_i^2 + \Delta K} \left[\left(\frac{5}{\ell} - 1, bv_{i+1}\ell\right)! - \left(\frac{5}{\ell} - 1, bv_i\ell\right)! \right]}{\sum_{i=0}^{n} \frac{A_i}{A_i^2 + \Delta K} \left[\left(\frac{3}{\ell}, bv_{i+1}\ell\right)! - \left(\frac{3}{\ell}, bv_i\ell\right)! \right]} \tag{15}$$

The advantage of this formulation is that for special argument ranges the incomplete factorial function may be approximated by very simple asymptotic expansions, thus facilitating computation.

The results of the numerical solution of equation (15) are illustrated by figure 14, where T_r is plotted as a function of Δ for various values of ℓ and for a particular value of the average electron energy $\langle U \rangle$. The value $\ell = 2$ represents the Maxwellian distribution function. When $\ell < 2$ the distribution becomes relatively rich in high energy particles. When $\ell > 2$ the distribution becomes rich in low energy particles relative to the Maxwellian distribution. The complete numerical results consist of several sets of curves like those shown in figure 1, each set corresponding to a different value of the mean electron energy $\langle U \rangle$.

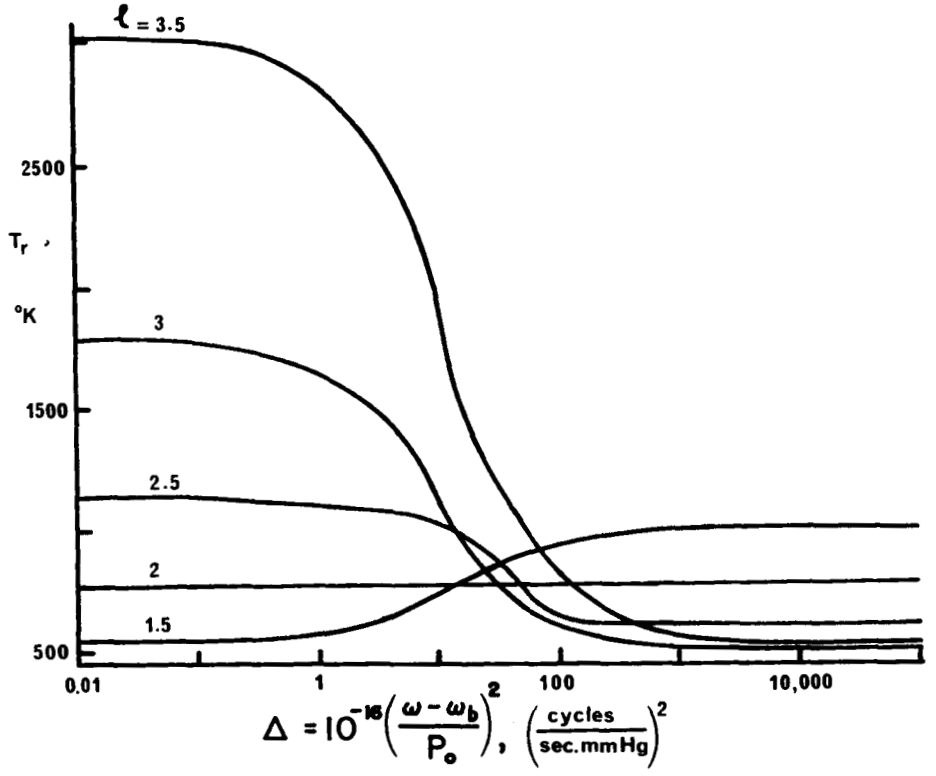

FIGURE 14. Typical Result of the Numerical Solution of the Equation Relating the Radiation Temperature (T_r) to the Frequency Parameter Δ. (Equation 15).

Experimental Results

The conduct of the experiment will be described by reference to figure 15. A repetitive discharge was established in the plasma cell at a rate of 100 pulses per second. A pulse duration of 10 microseconds was used. The input voltage and current to the cell were adjusted to provide an energy input of 50 millijoules per pulse. A typical set of values was 2000 volts and 2.5 amps.

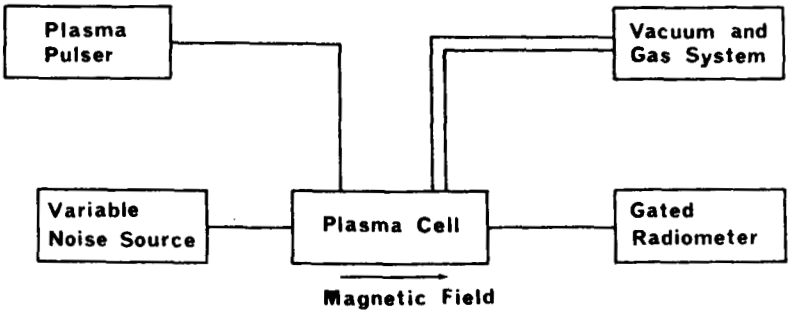

FIGURE 15. Schematic Diagram of the Experiment Used to Determine the Form of the Distribution Function in an Afterglow Plasma.

A gate time for the radiometer was selected. This determined the part of the afterglow plasma to be studied. Time equal to zero was defined as the terminating point of the voltage pulse that produced the active discharge. The magnitude of the longitudinal magnetic field was set at the desired value. The magnet power supply presently available limited the maximum field strength to 2700 gauss. This was not sufficient to allow an examination of the radiation intensity occurring when ω was equal to ω_b which required a field strength of 3200 gauss at the receiver frequency used. However a power supply with a 7000 gauss capability is due to be delivered shortly.

The radiometer is nulled by adjusting the precision attenuator in the variable noise source and the radiation temperature T_r is thereby determined (17).

After the magnetic field strength had been changed the radiometer was nulled again and this procedure was repeated until the variation of T_r as a function of Δ had been determined for this one particular time in the afterglow. The setting of the radiometer gate was then adjusted to a different time in the afterglow and a new plot of T_r vs. Δ was obtained. This procedure was repeated until the T_r vs. Δ plots for all desired times in the afterglow had been obtained.

The next step was to fit the experimental plots to the theoretical plots (of the type shown in figure 14) in order to determine how the values of ℓ and of the mean electron energy $\langle U \rangle$ vary during the afterglow period.

The results are shown in figures 16 and 17 which plot the values of the mean electron energy $\langle U \rangle$ and the exponential parameter ℓ, respectively, as functions of time in the afterglow.

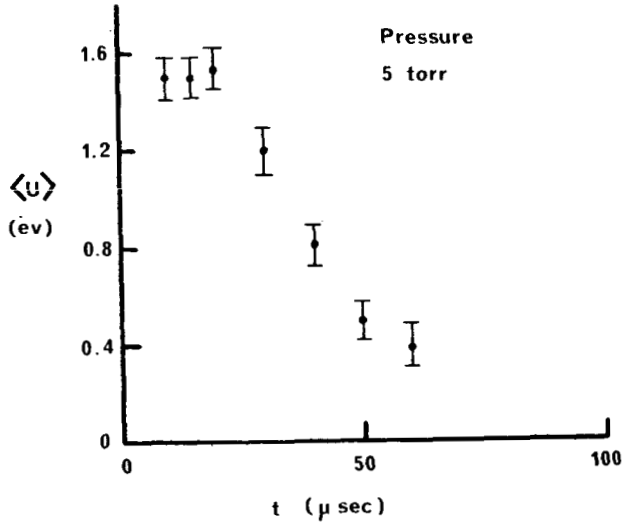

FIGURE 16. Experimental Result Showing the Variation of the Mean Electron Energy $\langle U \rangle$ as a Function of Time in the Afterglow.

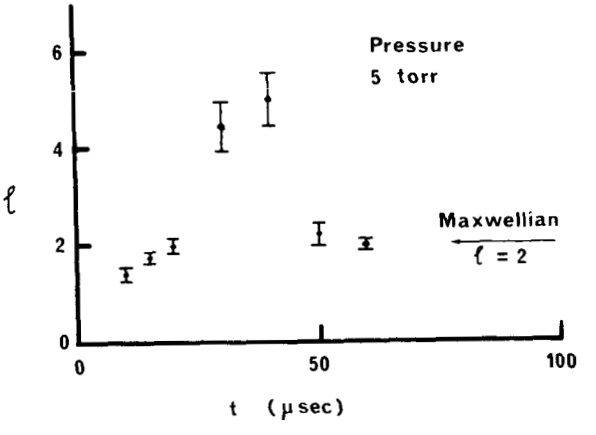

FIGURE 17. Experimental Result Showing the Variation of the Exponential Parameter ℓ as a Function of Time in the Afterglow.

We note that the mean electron energy remains high for 20 microseconds into the afterglow and that it has relaxed substantially towards the energy characteristic of a room temperature gas after 70 microseconds. In order to interpret figure 4 we bear in mind that a Maxwellian velocity distribution corresponds to a value of ℓ equal to 2. Thus in the first 20 microseconds $\ell < 2$ and the distribution maintains a populous high energy tail. From 20 to 70 microseconds $\ell > 2$ and the distribution contains more low energy electrons than is representative of the equilibrium state. By 70 microseconds into the afterglow the Maxwellian form is reached, although reference to figure 16 shows that the electron gas is still at a higher mean energy than its surroundings.

The anomalous behavior of the "temperature" of the electron gas which was previously reported (16) can now be understood by reference to figure 18. Here we compare the behavior of the radiation temperature T_r with that of the mean energy of the electron gas. Although the radiation temperature shows a rise to a maximum value during the afterglow period it is clear from the present study that this behavior is not mirrored by the mean energy of the electron gas but is, rather, due to the sharply varying form of the electron velocity distribution function in the early afterglow.

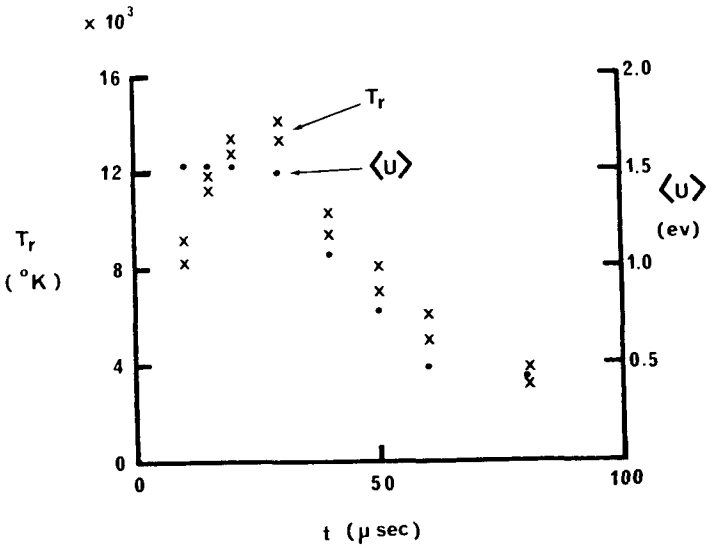

FIGURE 18. Plot of the "Anomalous" Rise of the Radiation Temperature T_r in the Afterglow Plasma in Comparison with the Behavior of the Mean Electron Energy.

PERSONNEL

Name	Position	Percent Time 1*	2*	3*
E. H. Holt	Professor Senior Investigator	50	75	50
H. B. Hollinger	Associate Professor	25	--	25
D. A. Huchital	Research Associate	(100)	100	100
H. Bayoumi	Graduate Assistant	(20)	100	Terminated Sept. 3, 1965
P. Blaszuk	Graduate Assistant	(20)	80	50
R. Jennings	Graduate Assistant	25	Terminated June 11, 1965	
P. N. Y. Pan	Graduate Assistant	37	80	50
R. M. Quinn	Graduate Assistant	50	100	50
J. A. Reynolds	Graduate Assistant	(20)	80	(20)
W. Taft	Research Assistant	--	50	--
Support Personnel				
H. Struss	Research Assistant (model shop)	50	50	10
J. Wright	Electronic Technician	100	100	100
W. Jennings	Student Technician	30	100	30
R. Ramachandran	Student Technician	30	50	Terminated Sept. 10, 1965
C. Cascio	Student Technician	30	100	30
H. Hanig	Student Technician	--	--	30 Commenced Oct. 4, 1965

Note

Figures in brackets indicate participation in the research without charge to the grant.

*1. May 1 - June 11, 1965

*2. June 14 - September 8, 1965

*3. September 9 - October 31, 1965

PLANS FOR THE NEXT PERIOD

Attention will be directed to the study of the different modes of the instability of the positive column. Special probe geometries will be used to distinguish between these modes. Microwave cavity techniques will be adapted to study density fluctuations. The work on non-Maxwellian velocity distributions will continue. Construction and testing of the remaining components of the cesium plasma cell will be completed.

During this period it is anticipated that the group will move to a new laboratory in the Materials Research Center at Rensselaer.

PAPERS PRESENTED

D. A. Huchital, E. H. Holt, Transport Phenomena in Ionized Gases as an Initial Value Problem. 7th International Conference on Phenomena in Ionized Gases, Belgrade, August, 1965.

CONTRACTOR REPORT PUBLISHED

R. A. Bitzer, E. H. Holt, A Microwave Lens System for Plasma Diagnostics, NASA CR-319, October 1965 (submitted as Technical Report No. 18 of the Plasma Research Laboratory).